


## Nematic reorientation effects on resonant modes, wavelength mismatch, and slow-light phenomena in one-dimensional magnetophotonic crystals with a dual anisotropic defect

E. J. Oliveira,<sup>1</sup> P. B. de Melo,<sup>1</sup> M. S. S. Pereira,<sup>1</sup> F. M. Zanetti,<sup>2</sup> and I. N. de Oliveira<sup>1</sup> 

<sup>1</sup>*Instituto de Física, Universidade Federal de Alagoas 57072-970 Maceió-AL, Brazil*

<sup>2</sup>*Departamento de Física, Universidade Federal do Paraná 81531-990 Curitiba-PR, Brazil*



(Received 12 April 2020; accepted 11 May 2020; published 26 May 2020)

The present study is devoted to the investigation of spectral properties of an alternated sequence of magnetic and dielectric layers containing a dual defect based on magnetic and nematic layers. Combining the Hydrodynamic Continuum Theory for nematic liquid crystals and Berreman's formalism, we determine how the nematic ordering affects the light localization, polarization rotation, and slow-light phenomena observed in the magnetophotonic system. In particular, we analyze the effects associated with a field-induced reorientation of the director in a nematic defect with strong planar boundary conditions. Our results reveal that field-induced reorientation of the nematic ordering can be used as an efficient mechanism to tune and control the spectral properties of magnetophotonic structure, anomalies in group velocity, and the wavelength mismatch between resonant mode and maximum polarization. The effects of nematic layer thickness are also analyzed.

DOI: [10.1103/PhysRevE.101.052704](https://doi.org/10.1103/PhysRevE.101.052704)

### I. INTRODUCTION

One-dimensional (1D) photonic crystals have been extensively studied in past decades due to their enormous potential for applications in optical devices, such as tunable filters [1–3], waveguides [4], and optical switches [5,6]. In particular, these systems correspond to a sequence of dielectric and/or metallic layers where some degree of periodicity can be found [7,8]. Such periodicity in the electrical response leads to a frequency range where the propagation of electromagnetic waves is prohibited. This frequency range is called the photonic band gap (PBG), in analogy to the electronic spectrum of crystalline solids. PBG characteristics can be adjusted accurately through appropriate manipulation of the periodic structure [9]. In addition, the introduction of disorder and defects in the photonic crystal architecture may be used to modify their spectral properties [10], thus leading to the emergence of localized modes within the photonic band gap. This rich phenomenology of photonic crystals already has been exploited in the design of optical microcircuits [11,12] and mirrorless lasers with low thresholds [13,14].

The introduction of magneto-optical layers into 1D photonic crystals gives rise to unique physical effects [15–17], which are associated with changes in the polarization state of the transmitted and reflected light beams. In particular, magneto-optical layers with a large optical activity are generally constituted of ferromagnetic or ferrimagnetic materials in their saturated magnetization states [18], thus exhibiting a dielectric tensor with complex off-diagonal elements. As a consequence, elliptically polarized light waves with opposite handedness exhibit different propagation velocities along these magnetic materials [18,19], resulting in a change in the polarization state of transmitted light that is denoted as Faraday rotation. In this context, multilayered systems containing magnetic layers are known as magnetophotonic

crystals, which present an enhanced Faraday rotation phenomenon due to the localization and multiple interference of propagating light through the periodic structure [20]. Because of the nonreciprocal character of the Faraday rotation, magnetophotonic crystals are widely used in the design of optical devices that require a high selectivity of polarization state of transmitted light, such as optical insulators [15,21] and spatial light modulators [22,23]. Furthermore, such a feature has been exploited in nonlinear optical phenomenon associated with some degree of symmetry breaking, such as second and third harmonic generation at resonant wavelengths of 1D magnetophotonic structures [16,17].

Recently several studies have been devoted to the investigation of the interplay between the nonreciprocal behavior of Faraday rotation and the nature of the birefringence in magnetophotonic photonic systems containing liquid crystal layers [24–31]. More specifically, it has been verified that the presence of nematic liquid crystals as regular layers of magnetophotonic structures introduces a new control parameter of spectral properties of such systems [24,25], corresponding to the relative orientation of the nematic director with respect to the propagation direction of the incident light beam. In particular, the electric control of the nematic director can be effectively used to tune and amplify the Faraday rotation effect in magnetophotonic systems, even in photonic architectures containing a single nematic layer as a central sole defect [25,28]. Moreover, the distinct Bragg resonances for the propagation eigenmodes for nematic and magnetic media lead to a wavelength mismatch between resonant modes and the maximum polarization rotation in 1D alternated sequences of linear or circular birefringent layers [30,31].

Although several theoretical studies have demonstrated that magnetophotonic structures containing multiple nematic layers are efficient systems for the polarization control of resonant modes, the experimental realization of such systems may

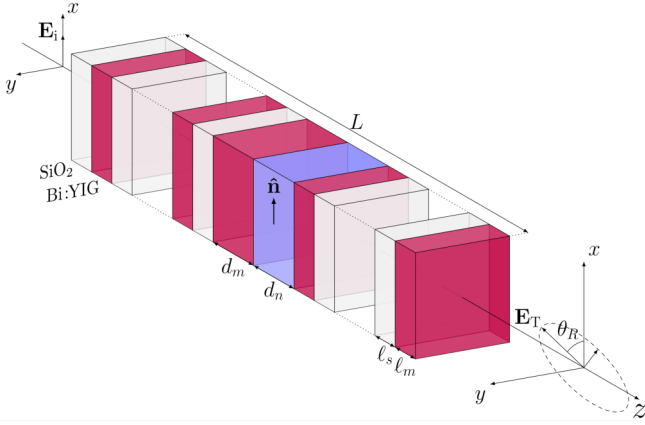


FIG. 1. Schematic representation of a multilayered structure consisting of an alternated sequence of SiO<sub>2</sub> dielectric (white) and Bi:YIG magnetic (red) layers, containing two central defects: one magnetic and the other nematic (purple). The unperturbed nematic director  $\hat{n}$  is parallel to the  $x$  axis. Here the thicknesses of both dielectric ( $\ell_s$ ) and magnetic ( $\ell_m$ ) layers are equal to 180 nm.

be a challenging task with a high cost of production. In this context, the present study is devoted to the analysis of spectral properties of a 1D multilayered structure, exhibiting a pair of defects: one magnetic and one nematic. Our results show that spectral properties of such a magnetophotonic crystal can be controlled by using an external electric field. In particular, we observe that the polarization rotation angle, transmittance of resonant modes, and group velocity can be tuned from the reorientation of the nematic director. The effects of nematic layer thickness are also analyzed.

## II. MODEL

We consider a magnetophotonic system consisting of an alternating sequence of dielectric (SiO<sub>2</sub>) and magneto-optical (Bi:YIG) layers, presenting magneto-optic and nematic defects as central layers, as represented in Fig. 1. The photonic structure presents a total of 32 layers, being organized as (SiO<sub>2</sub>/Bi:YIG/SiO<sub>2</sub>)<sup>*p*</sup>/*D<sub>m</sub>*/*D<sub>n</sub>*/(Bi:YIG/SiO<sub>2</sub>/Bi:YIG)<sup>*p*</sup>, where *D<sub>m</sub>* and *D<sub>n</sub>* are the magnetic and nematic defects of thicknesses *d<sub>m</sub>* and *d<sub>n</sub>*, respectively. *p* is the stacking number of the photonic structure, corresponding to the repetition number of the dielectric and magnetic subsets. In this case, the total number of layers of the structure is 6*p* + 2. The layers of SiO<sub>2</sub> present a thickness of  $\ell_s$ , while the regular layers of Bi:YIG exhibit a thickness  $\ell_m$ .

The transmission spectrum of the magnetophotonic structure for normal incidence can be computed when the refractive index and the thickness of the defects are varied. Following Berreman's 4 × 4 matrix numerical method [32], the propagation equation for light with angular frequency  $\omega$  is given by

$$\frac{d\psi(z)}{dz} = i\frac{\omega}{c}\Delta\psi(z), \quad (1)$$

where *c* is the light speed in vacuum and  $\psi(z)$  is a column vector with elements representing the *x*-*y* components of the electric *E* and magnetic *H* fields. Here we consider a uniform

medium in the *xy* plane, and  $\Delta$  is Berreman's matrix, which depends on the dielectric tensor of the material. We assume the regime of normal incidence for a propagation along the *z* axis, with the incident light beam presenting a polarization along the *x* axis. In this configuration, the Berreman's matrix is defined as

$$\Delta = \begin{pmatrix} 0 & 0 & 0 & 1 \\ 0 & 0 & -1 & 0 \\ \varepsilon_{yz}\frac{\varepsilon_{zx}}{\varepsilon_{zz}} - \varepsilon_{yx} & -\varepsilon_{yy} + \varepsilon_{yz}\frac{\varepsilon_{zy}}{\varepsilon_{zz}} & 0 & 0 \\ \varepsilon_{xx} - \varepsilon_{xz}\frac{\varepsilon_{zx}}{\varepsilon_{zz}} & \varepsilon_{xy} - \varepsilon_{xz}\frac{\varepsilon_{zy}}{\varepsilon_{zz}} & 0 & 0 \end{pmatrix}. \quad (2)$$

Here  $\varepsilon_{ij}$  are the components of the dielectric tensor of the propagation media, with  $(i, j) \in x, y, z$ .

In the nematic layer, the optical dielectric tensor depends on the director orientation in relation to the polarization on the incident light beam. The director vector is defined as  $\hat{n} = (\cos \alpha, 0, \sin \alpha)$ , with  $\alpha$  being the angle between the director and the *x* axis. The components of the optical dielectric tensor are given by  $\varepsilon_{ij} = \varepsilon_{\perp}^{\text{opt}}\delta_{ij} + (\varepsilon_{\parallel}^{\text{opt}} - \varepsilon_{\perp}^{\text{opt}})n_in_j$ . Here  $(i, j) \in x, y, z$ ; and  $\delta_{ij}$  is the Kronecker  $\delta$ .  $\varepsilon_{\parallel}^{\text{opt}}$  and  $\varepsilon_{\perp}^{\text{opt}}$  represent the optical dielectric permittivities of the liquid crystal layers, being defined in terms of the extraordinary and ordinary refractive indices:  $\varepsilon_{\parallel}^{\text{opt}} = n_e^2$  and  $\varepsilon_{\perp}^{\text{opt}} = n_o^2$ . Considering a nematic layer with planar boundary conditions, the director orientation may exhibit a spatial variation along the nematic layer when an external voltage is applied along the *z* direction, when its magnitude exceeds the threshold value  $V_{\text{th}} = \pi(K_1/\varepsilon_a)^{1/2}$ . *K<sub>1</sub>* is the splay elastic constant, and  $\varepsilon_a = \varepsilon_{\parallel} - \varepsilon_{\perp}$  corresponds to the static dielectric anisotropy, with  $\varepsilon_{\parallel}$  and  $\varepsilon_{\perp}$  being the static dielectric permittivities of the nematic sample. Depending on the amplitude of applied voltage, the orientation angle of the director may reach a maximum value  $\alpha_m$  at the center of nematic layer. In particular, the director orientation along the nematic layer can be determined from the minimization of the elastic energy in the Frank approach, being reasonably computed from the following pair of integral equations [33]:

$$\frac{V}{V_{\text{th}}} = \frac{2}{\pi}\sqrt{1 + \gamma\eta} \int_0^{\pi/2} f(\Gamma) d\Gamma, \quad (3)$$

$$\frac{2z}{d} = \frac{\int_0^{\sin^{-1}(\sin \alpha/\sqrt{\eta})} g(\Gamma) d\Gamma}{\int_0^{\pi/2} g(\Gamma) d\Gamma}, \quad (4)$$

where the parameters  $\Gamma$  and  $\eta$  are introduced from the relations  $\sin \alpha = \sin \alpha_m \sin \Gamma$  and  $\eta = \sin^2 \alpha_m$ . The functions  $f(\Gamma)$  and  $g(\Gamma)$  are given by

$$f(\Gamma) = \left[ \frac{1 + \kappa\eta \sin^2 \Gamma}{(1 + \gamma\eta \sin^2 \Gamma)(1 - \eta \sin^2 \Gamma)} \right]^{\frac{1}{2}} \quad (5)$$

and

$$g(\Gamma) = \left[ \frac{(1 + \gamma\eta \sin^2 \Gamma)(1 + \kappa\eta \sin^2 \Gamma)}{(1 - \eta \sin^2 \Gamma)} \right]^{\frac{1}{2}}. \quad (6)$$

Here  $\kappa = K_3/K_1 - 1$  defines the elastic anisotropy, and  $\gamma = \varepsilon_a/\varepsilon_{\perp}$ . *K<sub>1</sub>* and *K<sub>3</sub>* are the splay and bend elastic constants, respectively.  $\varepsilon_a$  and  $\varepsilon_{\perp}$  are the dielectric anisotropy and the perpendicular dielectric permittivity of the nematic sample for a static voltage. Equations (3) and (4) provide different profiles for the reorientation angle,  $\alpha(z)$ , depending on the

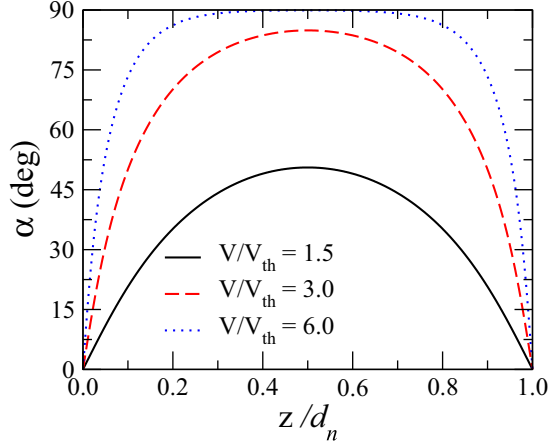


FIG. 2. Director orientation profile along a nematic layer with thickness  $d_n$ . The profiles correspond to the solutions of Eqs. (3) and (4) for distinct values of the applied external voltage:  $V/V_{th} = 1.5$  (black solid line),  $V/V_{th} = 3.0$  (red dashed line), and  $V/V_{th} = 6.0$  (blue dotted line). Due to the strong planar anchoring ( $\alpha(z=0) = \alpha(z=d_n) = 0$ ), one can note that the maximum value of the director tilt angle occurs at the center of the nematic defect, with  $\alpha_m \rightarrow \pi/2$  for  $V \gg V_{th}$ .

ratio between the applied and threshold voltages,  $V/V_{th}$ . More specifically, a uniform director occurs when  $V/V_{th} \leq 1$ , with  $\alpha(z) = 0$ . This situation indicates that the field contribution is not enough to overcome the high energy cost associated with the elastic distortion. On the other hand, a nonuniform director profile takes place for  $V/V_{th} > 1$ , as shown in Fig. 2. We used the typical parameters of 5CB liquid crystal, with  $K_1 = 6.2 \times 10^{-7}$  dyn,  $K_3 = 8.2 \times 10^{-7}$  dyn,  $\varepsilon_{\perp} = 7$ , and  $\varepsilon_{\parallel} = 18.5$  [34]. The strong planar anchoring conditions impose that the maximum value of the director tilt angle occurs at the center of the nematic defect, with  $\alpha_m \rightarrow \pi/2$  as the applied voltage becomes larger than the Freedericksz threshold  $V_{th}$ . As a consequence, a spatial variation of the optical dielectric tensor arises along the nematic layer. In what follows, we assume that the effects of optical electric field on the orientation nematic director are negligible.

For a magnetic layer presenting a magnetization along the direction of light propagation, the dielectric tensor is given by

$$\tilde{\varepsilon}_M = \begin{pmatrix} \varepsilon_1 & i\varepsilon_2 & 0 \\ -i\varepsilon_2 & \varepsilon_1 & 0 \\ 0 & 0 & \varepsilon_3 \end{pmatrix}, \quad (7)$$

where  $\varepsilon_2$  is the magnetic gyration, which exhibits a linear dependence on the material magnetization. The transversal components of  $\tilde{\varepsilon}_M$  are usually expressed in their complex form, with  $\varepsilon_1 = \varepsilon'_1 + i\varepsilon''_1$  and  $\varepsilon_2 = \varepsilon'_2 + i\varepsilon''_2$ . In particular, the real and imaginary components of  $\varepsilon_1$  and  $\varepsilon_2$  are associated with of the refractive index and the extinction coefficient of the magnetic materials [35].

The wave equation (1) can be solved through the Eidner-Oldano formalism [36], where  $\psi(z)$  is defined as the

superposition of four distinct plane waves

$$\psi(z) = \sum_{l=1}^4 C_l \psi^{(l)} e^{ik\lambda_l z}, \quad (8)$$

with  $\psi^{(l)}$  and  $\lambda_l$  corresponding, respectively, to the eigenvectors and the eigenvalues of the Berreman's matrix defined in Eq. (1). The components of the transmitted ( $T_x, T_y$ ) and reflected ( $R_x, R_y$ ) electric fields can be numerically determined from the solution of the following set of linear equations [32]:

$$\begin{aligned} E_x^i + R_x &= (F_{11} + F_{12}n_0)T_x + (F_{13} + F_{14}n_0)T_y, \\ (E_x^i - R_x)n_0 &= (F_{21} + F_{22}n_0)T_x + (F_{23} + F_{24}n_0)T_y, \\ E_y^i + R_y &= (F_{31} + F_{32}n_0)T_x + (F_{33} + F_{34}n_0)T_y, \\ (E_y^i - R_y)n_0 &= (F_{41} + F_{42}n_0)T_x + (F_{43} + F_{44}n_0)T_y, \end{aligned} \quad (9)$$

where  $E_x^i$  and  $E_y^i$  are the components of the incident electric field.  $F_{ij}$  correspond to the elements of the inverse transfer matrix, namely,  $F = \tau^{-1}$ , with  $\tau = \prod_{j=1}^{6p+2} \tau_j$ . Here  $\tau_j$  corresponds to the transfer matrix of the  $j$ th layer. In Eq. (9),  $n_0$  represents the refractive index of the incident medium, which is defined as the value of glass slides,  $n_0 = 1.5$ . The transmittance of the multilayered structure can be computed from the components of the transmitted electric field, with  $T = |T_x|^2 + |T_y|^2$ . The transmission coefficients can also be used to compute the polarization rotation angle  $\theta_R$ , ellipticity  $\xi$ , and the density of states (DOS)  $\rho(\omega)$  [37] as follows:

$$\theta_R = \frac{1}{2} \tan^{-1} \left[ \frac{2\text{Re}(T_y/T_x)}{1 - |T_y/T_x|^2} \right], \quad (10)$$

$$\xi = \frac{1}{2} \sin^{-1} \left[ -\frac{2\text{Im}(T_y/T_x)}{1 + |T_y/T_x|^2} \right], \quad (11)$$

$$\rho(\omega) = \frac{1}{L} \left| \frac{T_y \frac{dT_x}{d\omega} - T_x \frac{dT_y}{d\omega}}{T_y^2 + T_x^2} \right|, \quad (12)$$

where  $L$  is the total thickness of the film. The DOS can be used to obtain the group velocity  $v_{gr}$  of a wave packet, defined as  $v_{gr} = 1/\rho(\omega)$ . In what follows, we assume an incident wave presenting a linear polarization along the  $x$  axis. As the transmitted light may be elliptically polarized due to the birefringence of magneto-optic and nematic layers, the polarization rotation angle is determined from the relative direction between the major axis of the elliptical polarization and the  $x$  axis, as is represented in Fig. 1. Similarly, the ellipticity is defined as the ratio between minor and major axes of the elliptical polarization of the transmitted light.

### III. RESULTS

In Fig. 3 we present the density plot of transmittance spectra as a function of the nematic defect thickness,  $d_n$ , in the dual defect magnetophotonic structure, as shown in Fig. 1. We used  $\varepsilon_d = 2.01$  as the dielectric constant of silicon dioxide ( $\text{SiO}_2$ ). Typical parameters of 4'-*n*-pentyl-4-cyanobiphenyl (5CB) and bismuth-substituted yttrium iron garnet (Bi:YIG) were used as reference materials for the nematic and magnetic layers, respectively. In particular, we used  $\varepsilon_{\perp}^{\text{opt}} = n_o^2 (n_o = 1, 53)$ ,  $\varepsilon_{\parallel}^{\text{opt}} = n_e^2 (n_e = 1, 69)$ ,  $\varepsilon'_1 = 5, 59$ ,  $\varepsilon''_1 = 5, 42 \times 10^{-3}$ ,

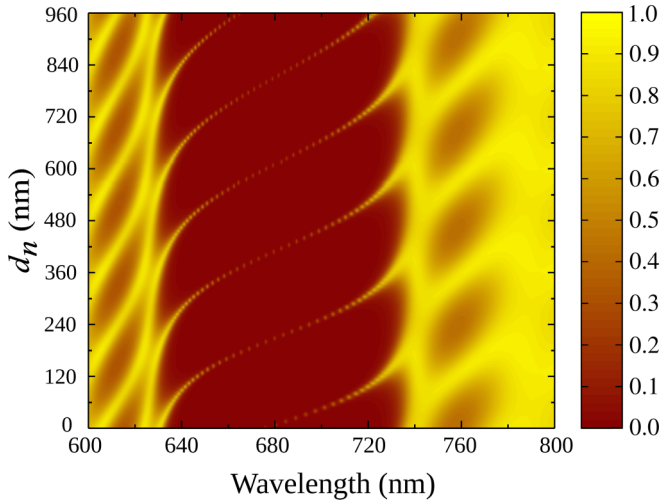


FIG. 3. Density plot of the transmission spectra of the dual defect magnetophotonic structure as a function of the nematic defect thickness,  $d_n$ . Here we consider a nematic defect presenting a director aligned along the  $x$  axis ( $V/V_{th} = 0$ ), with a birefringence  $\Delta n = 0.16$ . The thickness of the magnetic defect was maintained constant, with  $d_m = 2\ell_m$  and  $\ell_m = \ell_s = 180$  nm. Notice that the insertion of nematic defect modifies the light localization condition of the magnetophotonic structure for  $d_n > \ell_m/2$ , with the emergence of two distinct resonant modes inside the band gap.

$\varepsilon'_2 = -3,69 \times 10^{-3}$ , and  $\varepsilon''_2 = 2,08 \times 10^{-3}$ . We consider a multilayered structure with  $p = 5$ ,  $\ell_m = 180$  nm,  $\ell_s/\ell_m = 1$ , and  $d_m = 360$  nm, varying the thickness of nematic defect from 0 to 960 nm, in steps of 8 nm. The transmission spectra were computed for  $V/V_{th} = 0$ , corresponding to a uniform director profile along the nematic defect. One can note that the multilayered sequence presents a band gap centered at the red region of the electromagnetic spectrum, with a width that is independent on the thickness of the nematic layer. For  $d_n = 0$ , a single resonant mode is observed inside the band gap, being associated with the magneto-optical defect. Such a scenario is preserved as long  $d_n \ll \ell_m$ , with central magnetic and nematic layers behaving as a single defect with an effective thickness  $d_m + d_n$ . As the thickness of nematic defect is increased, the original resonant mode is shifted to the left border of the band gap and a second resonant mode emerges from the right border when  $d_n \geq \ell_m/2$ . Although the insertion of the nematic slab promotes a new break in the dielectric periodicity of the alternated sequence, such results show that the linear birefringence of the liquid-crystalline layer becomes relevant to the transmittance spectrum when  $d_n \geq \ell_m/2$ . Further, we observe a reduction in the wavelength shift between the two resonant modes as the nematic defect becomes larger than the magnetic one.

Figure 4(a) shows the effects of the nematic thickness on the polarization rotation angle of transmitted light by the magnetophotonic structure containing a dual defect. The same parameters as Fig. 3 were used, with  $V/V_{th} = 0$ . Similar to the resonant modes, the wavelength of maximum polarization rotation is strongly affected by the thickness of the nematic layer, with a red shift occurring as  $d_n$  increases. In fact, the polarization rotation peak is associated with the light

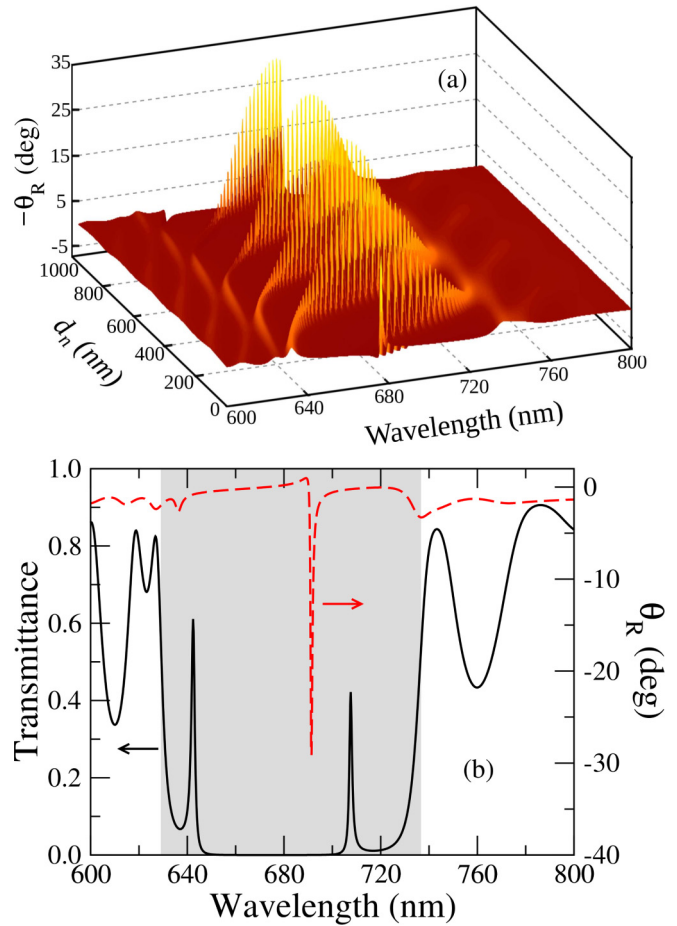


FIG. 4. (a) Polarization rotation angle of the transmitted wave by a 1D magnetophotonic structure containing a dual defect. We used the same parameters as Fig. 3, with  $d_m = 360$  nm. A pronounced enhancement of maximum polarization angle takes place as the thickness of the nematic defect is increased. (b) Wavelength mismatch between resonant modes in transmittance spectrum (black solid line) and polarization rotation angle (red dashed line), with  $d_m = 360$  nm and  $d_n = 480$  nm. The gray region marks the band gap width.

localization and multiple interference in the magnetic layers [20], being sensitive to changes in the light localization conditions. As a consequence, the maximum polarization rotation occurs for defect thicknesses in which the resonant modes are situated at the band gap center. Further, we notice a significant increase in the maximum polarization rotation angle as  $d_n$  is enlarged, indicating that the phase retardation induced by nematic birefringence provides an additional contribution to the changes in the polarization state of electromagnetic waves propagating through magnetophotonic crystals. However, the introduction of nematic defect induces a wavelength mismatch between the resonant modes and the polarization rotation peaks, which is attributed to the distinct propagation eigenmodes of electromagnetic waves for each defect layer [19,30]. Such a wavelength mismatch varies from 0 to 24 nm as the thickness of nematic layer is raised from 0 to 960 nm. In Fig. 4(b) we show the transmittance spectrum and polarization rotation angle for the magnetophotonic system with

$d_m = 360$  nm and  $d_n = 480$  nm, where the wavelength mismatch between resonant modes and polarization rotation peaks can be clearly observed. In particular, a huge rotation polarization takes place at  $\lambda_R = 690$  nm, which is shifted in relation to the resonant mode at  $\lambda_{D1} = 708$  nm. On the other hand, a very small polarization rotation is observed at  $\lambda = 637$  nm, which is slightly shifted in relation to the resonant mode at  $\lambda_{D2} = 643$  nm. Such a small polarization rotation may be associated with the interplay of linear and circular birefringence of nematic and magnetic layers, respectively. More specifically, the linear birefringence of nematic defect tends to induce a counterclockwise rotation in the direction polarization of an incident light, while the circular birefringence of magnetic layers leads to a clockwise rotation in the light polarization.

Let us now analyze the effects of an external applied voltage on the spectral properties of the multilayered structure presenting a dual defect. The density plot of transmittance spectra as a function of the applied voltage in nematic layer is presented in Fig. 5(a). We used the same parameters as Fig. 3, with  $d_n = 480$  nm. One can observe that the band gap is not affected by the applied voltage in the nematic defect, as is defined by the refractive indices and the thicknesses of regular layers in the photonic architecture. On the other hand, the wavelength and transmittance of resonant modes are strongly modified as the applied voltage is raised above the Fredericksz threshold,  $V_{th}$ . In particular, the field-induced reorientation of the nematic director modifies the effective refractive index,  $n_{eff}$  for an extraordinary wave propagating through the liquid crystalline defect, being defined as [38]

$$n_{eff} = \frac{1}{d_n} \int_0^{d_n} \frac{n_e n_o}{\sqrt{n_o^2 \cos^2 \alpha(z) + n_e^2 \sin^2 \alpha(z)}} dz. \quad (13)$$

As the applied voltage is raised well above the Fredericksz threshold, the maximum tilt angle tends to the asymptotic value of  $\pi/2$ , with  $n_{eff} \rightarrow n_o$ . As a consequence, the field-induced reorientation leads to a strong reduction of the nematic birefringence in the  $xy$  plane for  $V \gg V_{th}$ . In this situation, the nematic defect behaves as an isotropic dielectric layer with a refractive index  $n_o$ , changing the resonance conditions for defect modes inside the band gap. In Fig. 5(b) the transmittance of resonant modes as a function of the applied voltage is presented, considering a nematic defect with  $d_n = 480$  nm. Here we note that the applied voltage can be properly used to switch the mode with highest transmittance. Indeed, the applied voltage affects the position of resonant modes in relation to the band gap center, with the highest transmittance occurring for the resonant mode closest to one of the band edges.

In Fig. 6 we show the dependence of polarization rotation angle on the applied voltage in the nematic defect, with  $d_n = 480$  nm. For  $V < V_{th}$ , the nematic director stays aligned along the  $x$  axis, with polarization rotation angles remaining constant in this configuration. Due to the wavelength mismatch, a pronounced polarization rotation is observed close to the wavelength of the first resonant mode ( $\lambda_{D1}$ ), while a small polarization rotation is verified in the vicinity of the second resonant mode ( $\lambda_{D2}$ ). As the applied voltage is raised above the Fredericksz threshold, it is noticed a gradual

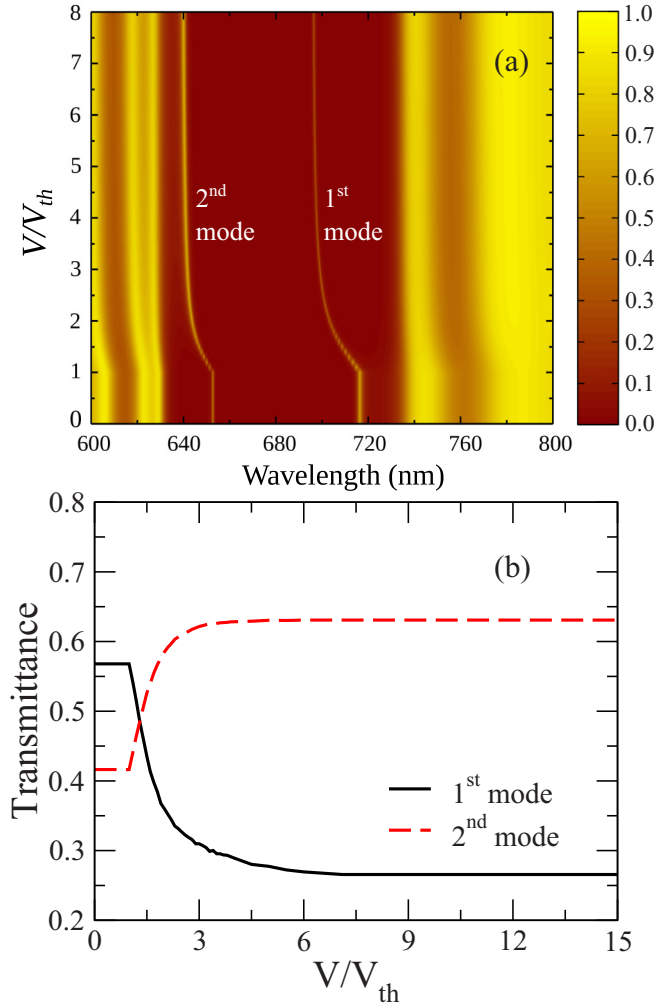


FIG. 5. (a) Density plot of the transmission spectra of the dual defect magnetophotonic structure as a function of the applied voltage in the nematic layer, with  $d_n = 480$  nm. We used the same parameters as Fig. 3. For  $V > V_{th}$ , we observe that the director reorientation modifies the Bragg conditions of resonant modes, being characterized by a wavelength shift and transmittance change of modes. (b) Transmittance of resonant modes as function of the applied voltage in the nematic defect, with  $d_n = 480$  nm. Notice that the applied voltage can be used to switch the mode with highest transmittance.

reduction in polarization rotation angle associated with the first resonant mode, reaching a constant value as the nematic director is reorientated along the field direction and  $n_{eff} \rightarrow n_o$ . A distinct scenario is observed for the polarization rotation angle associated with the second resonant mode, where a small increase of the polarization rotation takes places as  $\alpha_m \rightarrow \pi/2$ . Unlike the resonant modes, we observe that the field-induced reorientation of the nematic director does not change the wavelengths where the polarization rotation peaks take place. As a consequence, the wavelength mismatch is suppressed as  $V \gg V_{th}$ .

In order to provide a broader analysis of the polarization state of resonant modes, we exhibit the ellipticity spectra of the magnetophotonic structure in Fig. 7(a). We consider

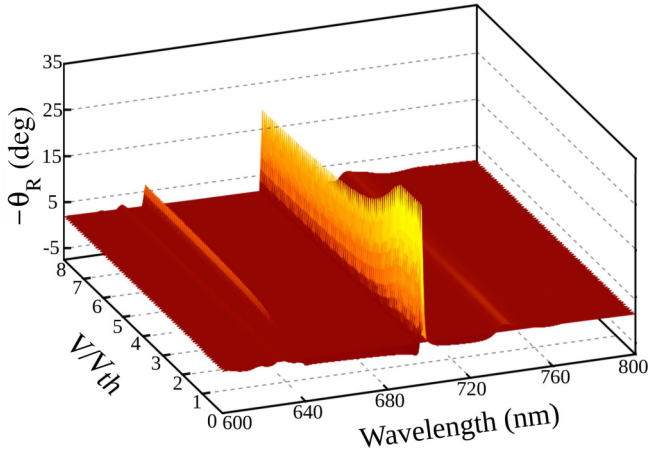


FIG. 6. Polarization rotation angle as function of the applied voltage in the nematic defect. The same parameters as Fig. 3 were used, with  $d_n = 480$  nm and  $\Delta n = 0.16$ . We observe a pronounced reduction of the polarization rotation angle associated with the first resonant mode, which is accompanied by a small increase of the polarization rotation angle associated with second resonant mode.

different values of the applied voltage in the nematic layer. Again the thicknesses of the magnetic and nematic layers are fixed, with  $d_m = 360$  nm and  $d_n = 480$  nm. For  $V/V_{th} = 0$ , we notice that  $\xi$  exhibits an asymmetric peak ( $\xi_P$ ) and valley ( $\xi_V$ ) signature close to the wavelength where the maximum polarization rotation occurs ( $\lambda_R = 690$  nm) [39–41], being associated with the distinct Bragg conditions for the propagation eigenmodes with opposite handedness. Such a peak-valley signature presents a similar behavior of the polarization rotation angle, being mismatched in relation to the defect wavelength,  $\lambda_{D1} = 708$  nm. In fact, the ellipticity degree is almost null at  $\lambda_{D1}$ , while small values of  $\xi$  take place close to the defect mode at  $\lambda_{D2} = 643$  nm. As a consequence, the resonant modes are linearly polarized along the  $x$  axis for  $V/V_{th} \leq 1$ . As the applied voltage is raised above the Freedericksz threshold, we observe that the reorientation of the nematic director promotes a considerable reduction in the values of  $\xi_P$  and  $\xi_V$ , indicating that the nematic orientation plays an important role in the polarization state of the resonant modes. As the wavelength mismatch is suppressed when  $V/V_{th} \gg 1$ , the resonant modes tend to acquire a slightly elliptical polarization due to the director reorientation. In Fig. 7(b) we present the ellipticity peak-valley difference,  $\Delta\xi_{P-V} = \xi_P - \xi_V$ , as function of the applied voltage. One can notice that  $\Delta\xi_{P-V}$  is gradually reduced as the applied voltage is increased, with  $\Delta\xi_{P-V}$  reaching a constant value in the limit  $V/V_{th} \gg 1$ . The inset shows the reduction of  $\xi_P$  and  $\xi_V$  as the applied voltage is increased.

Figure 8 shows the group velocity spectra of the magnetophotonic crystal with a dual defect, considering different applied voltages on the nematic layer. Again we used the parameters of Fig. 3, with  $d_n = 480$  nm. For  $V/V_{th} = 0$ , the group velocity is almost null at two wavelengths corresponding to the resonant modes, due to the divergence of the photonic density of states. Further, one can notice the occurrence of an anomaly in the group velocity at the wavelength corresponding to the maximum polarization rotation. Such an

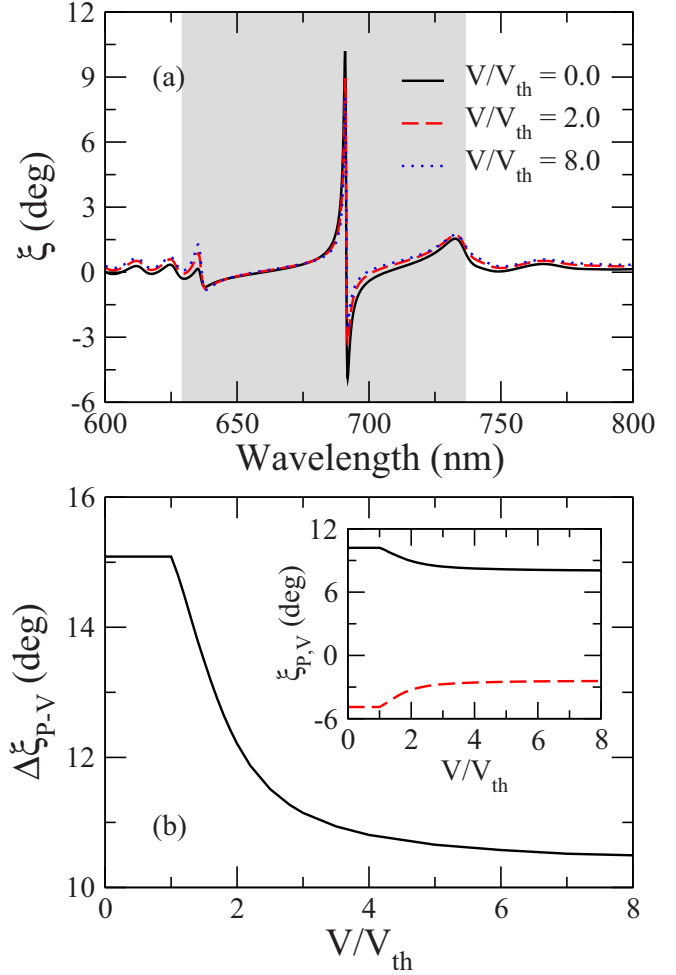


FIG. 7. (a) Ellipticity of the transmitted light by a 1D magnetophotonic structure containing a dual defect, considering different applied voltages on the nematic layer:  $V/V_{th} = 0$  (black solid line),  $V/V_{th} = 2$  (red dashed line),  $V/V_{th} = 8$  (blue dotted line). We used the same parameters as Fig. 3, with  $d_m = 360$  nm and  $d_n = 480$  nm. The gray region marks the band gap width. Notice that the nematic reorientation reduces the peak and valley amplitudes of the ellipticity close to the wavelength where the maximum polarization rotation occurs,  $\lambda_R = 690$  nm. (b) Voltage dependence of the ellipticity peak-valley difference,  $\Delta\xi_{P-V} = \xi_P - \xi_V$ . The inset shows the reduction of  $\xi_P$  (black solid line) and  $\xi_V$  (red dashed line) as the applied voltage is raised above the Freedericksz threshold.

anomaly seems to be directly associated with the mismatch between wavelength positions of resonant modes and maximum polarization rotations. For  $V/V_{th} = 2$ , we observe that the divergence of  $v_{gr}/c$  occurs in a wavelength very close to the resonant mode. As the applied voltage is raised well above the Freedericksz threshold ( $V/V_{th} = 8$ ), the anomaly is suppressed, with the divergence of  $v_{gr}/c$  being replaced by a pronounced reduction of group velocity at the resonant mode wavelength. In this case, the divergence of  $v_{gr}/c$  holds while the wavelength mismatch is non-null. However, it is important to emphasize that the divergence of  $v_{gr}/c$  occurs for wavelengths where the transmittance is null. The above results show that the field-induced reorientation of the nematic

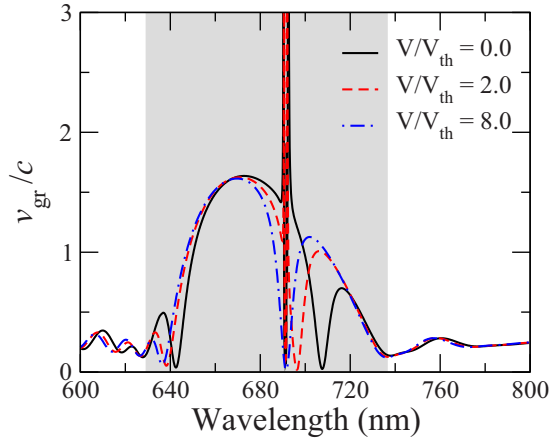


FIG. 8. Group velocity spectra (in units of  $c$ ) of magnetophotonic crystal with a dual defect, considering different applied voltages on the nematic layer:  $V/V_{th} = 0$  (black solid line),  $V/V_{th} = 2$  (red dashed line), and  $V/V_{th} = 8$  (blue dashed-dotted line). The gray region marks the band gap width. Notice that an anomaly on the group velocity takes place due to the mismatch between wavelength positions of resonant modes and maximum polarization rotations.

director can be used to tune minimum and maximum of group velocities of a light wave packet propagating through a magnetophotonic structure presenting magnetic and nematic layers as a dual defect. Such a behavior is particularly interesting in development of slow-light devices, such as optimized solar cells [42], label-free biosensors [43], and electro-optic modulators [44].

#### IV. SUMMARY AND CONCLUSIONS

In summary, we investigated the spectral properties of an alternated sequence of magnetic and dielectric layers, containing a dual defect based on magnetic and nematic layers. Combining the Hydrodynamic Continuum Theory for nematic liquid crystals and Berreman's formalism, we determined how the nematic ordering affects the light localization, polarization rotation, and slow-light phenomena observed in the magnetophotonic system. In particular, we analyzed the effects associated with a field-induced reorientation of the

director in a nematic defect with strong planar boundary conditions. Our results revealed that the linear birefringence of the nematic layer becomes relevant for spectral properties of the multilayered structure when its thickness becomes comparable to that of regular layers. Otherwise, the central magnetic and nematic layers behave as a single defect, with an effective thickness  $d_m + d_n$ . For  $d_n \geq \ell_m/2$ , we noticed that a second resonant mode emerges inside the photonic band gap in addition to the resonant mode associated with the central magnetic defect. However, a pronounced wavelength mismatch takes place between the wavelength positions of resonant modes and maximum polarization rotation, due to the distinct propagation eigenmodes of electromagnetic waves for each defect layer. Concerning the effects associated with an external electric field, we showed that the reorientation of the nematic director can be used as an efficient mechanism to tune resonant modes inside the photonic band gap, reducing the typical wavelength mismatch observed in 1D photonic structures based on materials presenting circular and linear birefringence. Further, we verified that the introduction of a nematic defect may give rise to anomalies in the group velocity spectra, being characterized by the divergence of group velocity at the wavelength of maximum polarization rotation. On the other hand, slow-light phenomena were observed at wavelengths corresponding to the resonant modes, which can be suitably tuned by the external electric field. In particular, we verified that the anomalies in the group velocity spectra vanish as the applied electric field is raised well above the Fredericksz threshold, accompanying the suppression of the wavelength mismatch between resonant modes and maximum polarization rotation. Our results showed that magnetophotonic structures containing a dual defect exhibit a rich phenomenology, which can be exploited in the design of new optical devices, such as optimized solar cells [42], label-free biosensors [43], and electro-optic modulators [44].

#### ACKNOWLEDGMENTS

This work was partially supported by INCT-FCx CNPq/MCT, CAPES, and FINEP (Brazilian Research Agencies), as well as FAPEAL (Alagoas State Research Agency).

- [1] K. L. Jim, D. Y. Wang, C. W. Leung, C. L. Choy, and H. L. W. Chan, *J. Appl. Phys.* **103**, 083107 (2008).
- [2] H. Němec, L. Duvillaret, F. Garet, P. Kužel, P. Xavier, J. Richard, and D. Raully, *J. Appl. Phys.* **96**, 4072 (2004).
- [3] Y.-J. Xiang, X. Dai, S.-C. Wen, and D.-Y. Fan, *Opt. Lett.* **33**, 1255 (2008).
- [4] H. Taniyama, *J. Appl. Phys.* **91**, 3511 (2002).
- [5] G. Ma, J. Shen, Z. Zhang, Z. Hua, and S. H. Tang, *Opt. Express* **15**, 858 (2006).
- [6] A. E. Miroshnichenko, E. Brasselet, and Y. S. Kivshar, *Appl. Phys. Lett.* **92**, 253306 (2008).
- [7] S. John, *Phys. Rev. Lett.* **58**, 2486 (1987).
- [8] E. Yablonovitch, *Phys. Rev. Lett.* **58**, 2059 (1987).
- [9] J. D. Joannopoulos, P. R. Villeneuve, and S. Fan, *Nature (London)* **386**, 143 (1997).
- [10] Y. Lahini, A. Avidan, F. Pozzi, M. Sorel, R. Morandotti, D. N. Christodoulides, and Y. Silberberg, *Phys. Rev. Lett.* **100**, 013906 (2008).
- [11] S. Lan, K. Kanamoto, T. Yang, S. Nishikawa, Y. Sugimoto, N. Ikeda, H. Nakamura, K. Asakawa, and H. Ishikawa, *Phys. Rev. B* **67**, 115208 (2003).
- [12] E. H. E. Boudouti, Y. E. Hassouani, H. Aynaou, B. Djafari-Rouhani, A. Akjouj, and V. R. Velasco, *J. Phys.: Condens. Matter* **19**, 246217 (2007).
- [13] S. Noda, M. Imada, M. Okano, S. Ogawa, M. Mochizuki, and A. Chutinan, *IEEE J. Quantum Electron.* **38**, 726 (2002).
- [14] K. Shin, M. H. Song, B. Park, T. Ohta, Y. Tsunoda, H. Hoshi, Y. Takanishi, K. Ishikawa, J. Watanabe, S. Nishimura *et al.*, *Adv. Mater.* **16**, 779 (2004).

- [15] M. Inoue, R. Fujikawa, A. Baryshev, A. Khanikaev, P. B. Lim, H. Uchida, O. Aktsipetrov, A. Fedyanin, T. Murzina, and A. Granovsky, *J. Phys. D* **39**, R151 (2006).
- [16] O. A. Aktsipetrov, T. V. Dolgova, A. A. Fedyanin, T. V. Murzina, M. Inoue, K. Nishimura, and H. Uchida, *J. Opt. Soc. Am. B* **22**, 176 (2005).
- [17] T. V. Murzina, E. M. Kim, R. V. Kapra, I. V. Moshnina, O. A. Aktsipetrov, D. A. Kurdyukov, S. F. Kaplan, and V. G. Golubev, *Appl. Phys. Lett.* **88**, 022501 (2006).
- [18] A. K. Zvezdin and V. A. Kotov, *Modern Magneto-optics and Magneto-optical Materials* (Institute of Physics Publishing, Bristol, 1997).
- [19] M. Levy, *J. Appl. Phys.* **99**, 073104 (2006).
- [20] M. Inoue, K. Arai, T. Fujii, and M. Abe, *J. Appl. Phys.* **85**, 5768 (1999).
- [21] M. Zamani, M. Ghanaatshoar, and H. Alisafae, *J. Opt. Soc. Am. B* **28**, 2637 (2011).
- [22] S. Kharratian, H. Urey, and M. C. Onbasli, *Sci. Rep.* **9**, 644 (2019).
- [23] S. Kharratian, H. Urey, and M. C. Onbasli, *Adv. Opt. Mater.* **8**, 1901381 (2020).
- [24] H.-X. Da, Z.-Q. Huang, and Z. Y. Li, *Opt. Lett.* **34**, 1693 (2009).
- [25] H.-X. Da, Z.-Q. Huang, and Z. Y. Li, *Opt. Lett.* **34**, 356 (2009).
- [26] H. X. Da, P. Xu, J. C. Wu, and Z. Y. Li, *J. Appl. Phys.* **104**, 033911 (2008).
- [27] H.-X. Da, Z.-Q. Huang, and Z.-Y. Li, *J. Appl. Phys.* **108**, 063505 (2010).
- [28] S. Keramati, M. Zamani, and M. Ghanaatshoar, *J. Appl. Phys.* **114**, 023101 (2013).
- [29] J. Luo, P. Xu, and L. Gao, *Solid State Commun.* **151**, 993 (2011).
- [30] R. R. da Silva, F. M. Zanetti, and I. N. de Oliveira, *Phys. Rev. E* **89**, 012508 (2014).
- [31] E. J. Oliveira, P. B. de Melo, R. R. da Silva, F. M. Zanetti, and I. N. de Oliveira, *J. Appl. Phys.* **124**, 113103 (2018).
- [32] D. W. Berreman, *J. Opt. Soc. Am.* **62**, 502 (1972).
- [33] I. C. Khoo, *Liquid Crystals: Physical Properties and Nonlinear Optical Phenomena* (Wiley-Interscience, New York, 1994).
- [34] D. A. Dunmur, A. Fukuda, and G. R. Luckhurst, *Physical Properties of Liquid Crystals: Nematics* (Inspec, London, 2001).
- [35] H. Kato, T. Matsushita, A. Takayama, and M. Egawa, *J. Appl. Phys.* **93**, 3906 (2003).
- [36] S. Stallinga, *J. Appl. Phys.* **85**, 3023 (1999).
- [37] J. M. Bendickson, J. P. Dowling, and M. Scalora, *Phys. Rev. E* **53**, 4107 (1996).
- [38] T. Scharf, *Polarized Light in Liquid Crystals and Polymers* (Wiley-Interscience, New York, 2001).
- [39] A. H. Gevorgyan, *Opt. Spectrosc.* **106**, 43 (2009).
- [40] C. P. Yin, T. B. Wang, and H. Z. Wang, *Eur. Phys. J. B* **85**, 104 (2012).
- [41] T. Goto and M. Inoue, *J. Appl. Phys.* **111**, 07A913 (2012).
- [42] O. Deparis and O. E. Daif, *Opt. Lett.* **37**, 4230 (2012).
- [43] K. Qin, S. Hu, S. T. Retterer, I. I. Kravchenko, and S. M. Weiss, *Opt. Lett.* **41**, 753 (2016).
- [44] H. Yan, X. Xu, C.-J. Chung, H. Subbaraman, Z. Pan, S. Chakravarty, and R. T. Chen, *Opt. Lett.* **41**, 5466 (2016).